npj | climate and atmospheric science

www.nature.com/npjclimatsci

ARTICLE OPEN

Check for updates

Changes in Hadley circulation and intertropical convergence zone under strategic stratospheric aerosol geoengineering

Wei Cheng[1,2]✉, Douglas G. MacMartin[3]✉, Ben Kravitz[4,5], Daniele Visioni[3], Ewa M. Bednarz[3], Yangyang Xu[6], Yong Luo[7], Lei Huang[7], Yongyun Hu[8], Paul W. Staten[4], Peter Hitchcock[9], John C. Moore[10,11,12], Anboyu Guo[13] and Xiangzheng Deng[1,2,14]✉

Stratospheric aerosol geoengineering has been proposed as a potential solution to reduce climate change and its impacts. Here, we explore the responses of the Hadley circulation (HC) intensity and the intertropical convergence zone (ITCZ) using the strategic stratospheric aerosol geoengineering, in which sulfur dioxide was injected into the stratosphere at four different locations to maintain the global-mean surface temperature and the interhemispheric and equator-to-pole temperature gradients at present-day values (baseline). Simulations show that, relative to the baseline, strategic stratospheric aerosol geoengineering generally maintains northern winter December–January–February (DJF) HC intensity under RCP8.5, while it overcompensates for the greenhouse gas (GHG)-forced southern winter June–July–August (JJA) HC intensity increase, producing a 3.5 ± 0.4% weakening. The residual change of southern HC intensity in JJA is mainly associated with stratospheric heating and tropospheric temperature response due to enhanced stratospheric aerosol concentrations. Geoengineering overcompensates for the GHG-driven northward ITCZ shifts, producing 0.7° ± 0.1° and 0.2° ± 0.1° latitude southward migrations in JJA and DJF, respectively relative to the baseline. These migrations are affected by tropical interhemispheric temperature differences both at the surface and in the free troposphere. Further strategies for reducing the residual change of HC intensity and ITCZ shifts under stratospheric aerosol geoengineering could involve minimizing stratospheric heating and restoring and preserving the present-day tropical tropospheric interhemispheric temperature differences.

npj Climate and Atmospheric Science (2022)5:32 ; https://doi.org/10.1038/s41612-022-00254-6

INTRODUCTION

The Hadley cell (HC) is a large-scale atmospheric circulation feature driven by differential heating of the Earth's surface. It consists of warm moist air ascending in the Intertropical Convergence Zone (ITCZ) and diverging poleward in the upper troposphere, and cool and dry air descending in the subtropical zone and converging in the lower troposphere, and it plays an important role in forming tropical and subtropical climatic zones, especially the locations of the deserts[1]. HC shapes the distribution of the Earth's surface's dry and wet regions by influencing the distributions of precipitation, relative humidity, and clouds[2]. Mamalakis et al.[3] showed that zonally contrasting shifts of the tropical rain belt with climate change, could affect agricultural productivity and food security of billions of people[4].

Observational evidence shows a poleward expansion of the HC in the past few decades[5,6]. Climate model simulations with increased greenhouse gas (GHG) forcing also indicate a poleward expansion of the HC[7–9]. A noticeable weakening of the annually averaged intensity of the HC under global warming has been reported by several studies[10,11]. Vallis et al.[12] analyzed the response of CMIP5 climate models, finding a weakening of HC in most models in the winter season is largely confined to the Northern hemisphere with global warming. Approximately half of the models predict a strengthening of the Southern hemisphere HC during June–July–August (JJA), though the other half exhibits a weakening[13]. Seo et al.[13] found that a change in the meridional temperature gradients is a dominant factor for change in HC strength in a warming climate, using two scaling relations based on Held and Hou[14], and Held[15]. In general, the slowdown of the tropical large-scale circulation in a warming climate is associated with a weakening of convective mass flux caused by increased dry static stability and reduced meridional surface temperature gradients in the tropics and subtropics[11,16,17].

The ITCZ is a planetary-scale band of heavy precipitation close to the equator. Under a warming climate, the narrowing of ITCZ appears in both observations[18] and climate models[1,19]. The magnitude of the ITCZ narrowing is highly related to the gross moist stability and tropical clouds in a warming climate[20]. ITCZ migrations can be induced by hemispherically asymmetric changes in the extratropics, e.g., tropospheric aerosol forcing[21] or the Atlantic meridional overturning circulation energy transport[22,23]. Seasonally, the ITCZ migrates towards the warmer hemisphere, its position is determined by nonlinear meridional advection of angular momentum and ocean thermal inertia[24], and

[1]Institute of Geographic Sciences and Natural Resources Research, Chinese Academy of Sciences, Beijing, China. [2]Key Laboratory of Land Surface Pattern and Simulation, Chinese Academy of Sciences, Beijing, China. [3]Mechanical and Aerospace Engineering, Cornell University, Ithaca, NY, USA. [4]Department of Earth and Atmospheric Sciences, Indiana University, Bloomington, IN, USA. [5]Atmospheric Sciences and Global Change Division, Pacific Northwest National Laboratory, Richland, WA, USA. [6]Department of Atmospheric Sciences, Texas A&M University, College Station, TX, USA. [7]Department of Earth System Science, Ministry of Education Key Laboratory for Earth System Modeling, Institute for Global Change Studies, Tsinghua University, Beijing, China. [8]Laboratory for Climate and Ocean-Atmosphere Sciences, Department of Atmospheric and Oceanic Sciences, School of Physics, Peking University, Beijing, China. [9]Department of Earth and Atmospheric Science, Cornell University, Ithaca, NY, USA. [10]College of Global Change and Earth System Science, Beijing Normal University, Beijing, China. [11]CAS Center for Excellence in Tibetan Plateau Earth Sciences, Beijing, China. [12]Arctic Centre, University of Lapland, Rovaniemi, Finland. [13]National Marine Environmental Forecasting Center, Ministry of Natural Resources, Beijing, China. [14]University of Chinese Academy of Sciences, Beijing, China.
✉email: chengwei@igsnrr.ac.cn; dgm224@cornell.edu; dengxz@igsnrr.ac.cn

Table 1. Summary of the simulations analyzed in this study, the climate objectives, and the degrees of freedom used[59,60].

Simulation name	Description
GLENS	Stratospheric sulfur injection at four latitudes, 30°N, 30°S, 15°N, and 15°S to maintain global-mean surface temperature (T0), the interhemispheric (south-to-north) temperature gradient (T1), and the equator-to-pole temperature gradient (T2) at 2010–2030 levels
GEQ	Stratospheric sulfur injection at the equator to maintain T0 at 2010–2030 levels
Solar3x3	Solar dimming in three independently adjusted patterns (globally uniform, linear with the sine of latitude, and quadratic with the sine of latitude) to maintain T0, T1, and T2 at 2010–2030 levels
Solar1x1	Uniform solar dimming to maintain T0 at 2010–2030 levels
GEOHEAT_S	No enhanced stratospheric aerosol concentrations but with added stratospheric heating derived from GLENS. 14 month simulations with annual mean climate variables from March of the first year to February of the second year.

ocean energy uptake by upwelling of cold waters[23]. Changes in tropical belt width and intensity are critically important for the hydrological system and hence for the habitability of several heavily-populated areas[1,16].

Stratospheric aerosol injection (SAI) geoengineering has been considered a possible way to mitigate the impacts of climate change due to rising GHG concentrations[25,26]. This idea gets its inspiration from the stratospheric aerosol layer formed from large volcanic eruptions, which cools the Earth's surface for several years[27]. SAI geoengineering can lessen the effect of global warming due to the increasing concentrations of GHG by reducing incoming solar radiation[28].

To date, few studies of the impact of geoengineering on the tropical atmospheric circulation have been published. Reduction in precipitation in both total amount and frequency of extremes indicates a considerable weakening of the hydrological cycle in solar dimming simulations conducted as part of the Geoengineering Model Intercomparison Project (GeoMIP), which is associated with differences in shortwave and longwave forcing impacts on atmospheric circulation[29]. Smyth et al.[30] indicated that GeoMIP G1 solar dimming geoengineering nearly restores preindustrial temperatures, but the global hydrology is altered and driven by shifts of the HC. They also noted damping of the seasonal migration of the ITCZ under solar dimming geoengineering, likely associated with preferential cooling of the summer hemisphere[30]. Guo et al.[31] found that the HC intensity in the winter cells and the seasonal migration of the ITCZ are reduced under geoengineering experiments with solar dimming. Using an intermediate complexity climate model, Ferraro et al.[32] found that geoengineering with stratospheric sulfate aerosol does not mitigate the weakening of the circulation under anthropogenic global warming. This was due to the tropospheric response to radiative heating from the aerosol layer placed in the lower stratosphere intended to return the global-mean surface temperature to the 20th-century baseline.

However, these past modeling studies have examined very idealized scenarios, typically with solar dimming as in the GeoMIP scenarios G1[33], or tropical injection scenarios, e.g., GeoMIP scenarios G3[33] and Ferraro et al.[32]. These scenarios are designed with the aim of offsetting changes in global-mean surface air temperature (T0). In contrast, maintaining interhemispheric surface air temperature difference (T1), and the equator-to-pole surface air temperature gradient (T2) can reduce some side effects that result from only offsetting change in T0 by geoengineering[34]. Controlling T1 is expected to reduce shifts in the latitude of the ITCZ and associated tropical precipitation that could occur if one hemisphere is cooled more than the other[35,36], while controlling T2 is motivated by the overcooling of the tropics relative to the poles that is seen in many previous studies, e.g., Bala & Caldeira[37]; Kravitz et al.[28,38].

Here, we focus on the HC intensity and ITCZ shift calculated via the meridional mass stream function under the strategic stratospheric sulfate aerosol geoengineering controlling three temperature-related metrics (T0, T1, and T2). We use the GLENS 20-member ensemble of simulations with a state-of-the-art climate model to estimate the forced response in the presence of natural variability, and a multiple-latitude injection strategy deliberately designed to reduce residual temperature changes[34]. Using an HC intensity scaling theory[13], we identify the driving factors determining changes in HC intensity under the strategic stratospheric aerosol geoengineering. We also investigate the ITCZ shift and associated contributing factors, e.g., tropical interhemispheric temperature gradients both in the surface and troposphere under strategic geoengineering. To better understand the responses of HC intensity and ITCZ shift to the strategic stratospheric sulfate aerosol geoengineering, we also compare our results to those from the only stratospheric aerosol equatorial injection, solar dimming, and stratospheric heating simulations (Table 1).

RESULTS

Temperature responses under geoengineering

Increased CO_2 concentrations under RCP8.5 raise the tropospheric temperature and lower that of the stratosphere. There is amplified warming over the higher latitudes, especially during the winter season, due to local positive feedback at the poles[39,40] (Fig. 1a, d). Geoengineering successfully maintains T0 and T1 at the baseline levels with SO_2 injections at four independent locations in GLENS and with only equatorial injection in GEQ[41]. In the Community Earth System Model, version 1, using the Whole Atmosphere Community Climate Model as its atmospheric component, CESM1 (WACCM)[42] (model description is in the Methods section), roughly uniformly distributed CO_2 warms the Northern Hemisphere more than the Southern Hemisphere, and the roughly hemispherically symmetric aerosol distribution from GEQ cools the Northern Hemisphere more than the Southern Hemisphere, resulting in effectively meeting the T1 goal even without specifying this goal. Only specifically targeting the equator-to-pole temperature gradient, as in GLENS, is effective at further reducing T2 changes relative to GEQ[34]. Relative to the baseline, both stratospheric aerosol geoengineering ensembles show some warming in the tropical lower stratosphere, some tropospheric overcooling, a decrease in the subtropical tropopause height, and some surface warming in winter at high latitudes.

Sulfate aerosols absorb (near-IR) shortwave radiation and change longwave emission[43], hence heating the stratosphere. In the GLENS simulations (offsetting ~4 °C of global warming under RCP8.5), the maximum stratospheric warming reaches 16 °C near the peak aerosol mass mixing ratio (not shown) at ~70 hPa[44,45]. Even though the latitudinal extent of the stratospheric heating is similar in both ensembles, GEQ results in ~60% more heating in the tropics than in GLENS due to more aerosol loading in the tropics (not shown)[46]. Both stratospheric aerosol geoengineering ensembles and the solar dimming experiments show some tropical tropospheric cooling. Relative to the baseline, in the

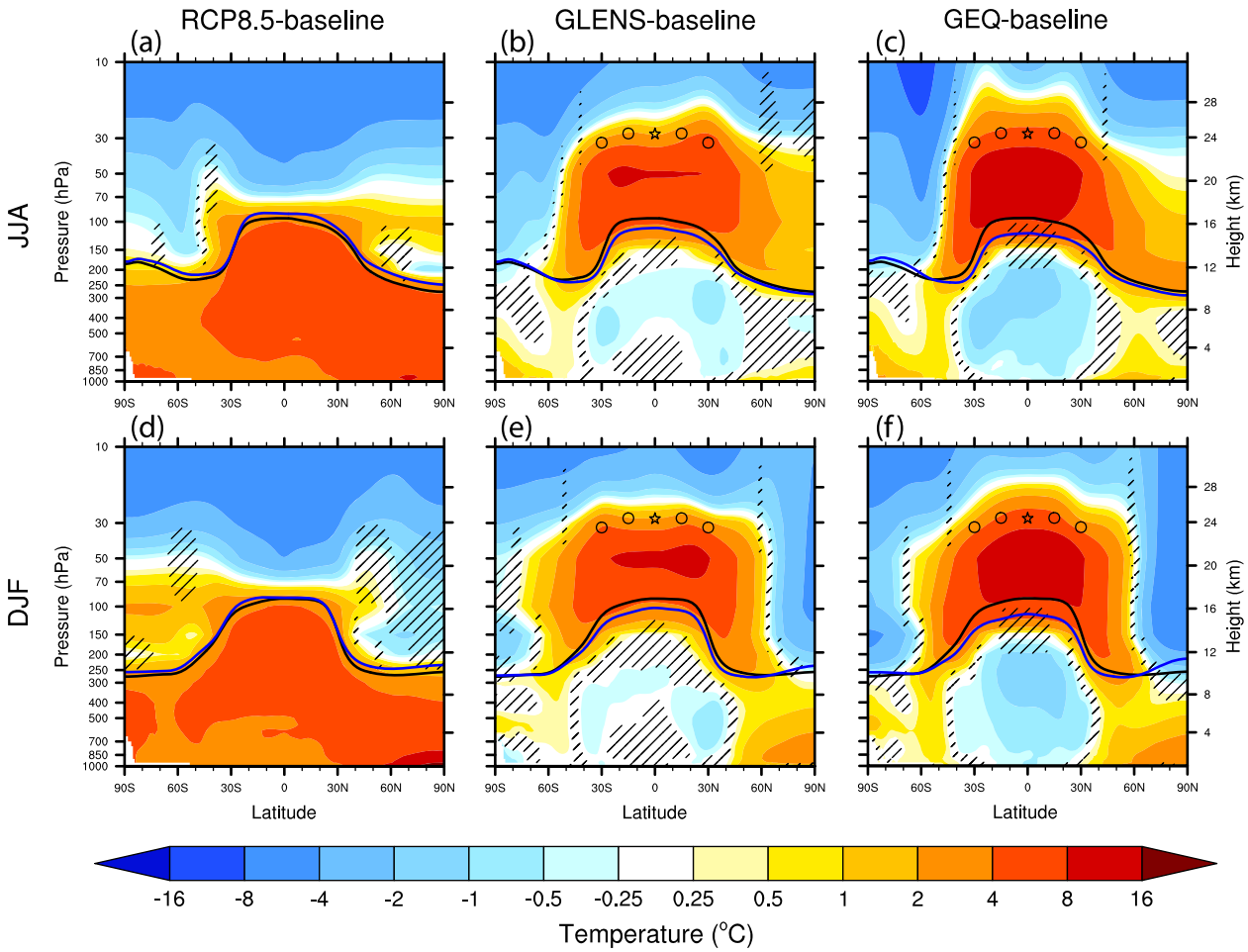

Fig. 1 Changes in zonally seasonal mean temperature. Changes in zonally averaged June–July–August (JJA, **a**–**c**), December–January–February (DJF, **d**–**f**) mean temperature (°C) in RCP8.5 (**a**, **d**), GLENS (**b**, **e**), and Equatorial injection (GEQ; **c**, **f**) ensemble mean averaged over the period 2075–2095, relative to RCP8.5 averaged over years 2010–2030 ensemble mean (Baseline). Hatched areas are regions where changes are not statistically significant at the 5% level using the Student's *t* test. The four circles indicate the four SO_2 injection locations in GLENS, and the star indicates the injection location in GEQ. The black solid line indicates the tropopause in the baseline, and the blue solid line indicates the tropopause in the perturbed experiment.

GEQ and Solar1x1 simulations, there is a statistically significant hemispherically asymmetric tropospheric (from surface to 200 hPa) overcooling ranging from 0.2 to 2 °C in the tropics (Fig. 1 and Supplementary Fig. 1). Geoengineering maintaining the three temperature-related metrics at the baseline by stratospheric sulfur injection or solar dimming produces a weaker tropospheric overcooling than aerosol or solar geoengineering just maintaining global-mean surface temperature, respectively. The overcooling is mostly located near 30° S/N in the middle of the troposphere for maintaining T0, T1, and T2 targets at the baseline under GLENS and Solar3x3. At boreal mid- and high latitudes of the Northern Hemisphere, moderate winter warming appears in both solar dimming geoengineering ensembles. There is some stronger residual tropospheric warming during winter under both aerosol geoengineering ensembles, especially at the surface, which resembles a classic winter warming signal after volcanic eruptions[47,48].

The residual tropospheric temperature changes under geoengineering are a consequence of differences in the seasonality and in the latitudinal and vertical structures of the CO_2 and sulfate aerosol forcings (e.g., Henry and Merlis[49]; Govindasamy et al.[50]). They are associated with changes in tropical static stability and meridional temperature gradient, which are quoted in Table 2 and Supplementary Table 1 for each geoengineering experiment together with associated standard errors. In the GEQ and Solar1x1 simulations, tropical static stability decreases by about 2.5 ± 0.2% and 4.2 ± 0.2% in December–January–February (DJF), respectively, relative to the baseline. In JJA, tropical static stability decreases by about 2.7 ± 0.2% in both GEQ and Solar1x1 (Table 2 and Supplementary Table 1). In GLENS and Solar3x3, seasonal changes in tropical static stability are smaller than in GEQ and Solar1x1, respectively, due to a smaller temperature contrast between 200 and 925 hPa in the tropics when maintaining three temperature-related metrics at the baseline. For the meridional temperature gradient, there is a 2.4 ± 0.8% and 3.8 ± 0.4% increase in JJA for GEQ and GLENS, respectively, relative to the baseline. The smaller change in a meridional temperature gradient in GEQ is associated with quantitively similar tropospheric overcooling near the equator and over 10–30°S, while in GLENS the tropospheric overcooling over 10–30°S is much stronger than near the equator. Changes in a meridional temperature gradient in JJA are not statistically significant under Solar3x3 and Solar1x1.

In DJF, the meridional temperature gradient increases by 1.2 ± 0.3% in GLENS. However, it decreases by 4.0 ± 0.6% and 4.4 ± 0.5% in GEQ and Solar1x1, respectively, which are both caused by stronger overcooling near the equator than the northern hemisphere subtropics (10–30°N average) and residual tropospheric warming at boreal midlatitudes. Compared with the baseline, the warming of the tropical stratosphere and the cooling of the troposphere result in ~10% reduction of subtropical tropopause

Table 2. June–July–August (JJA) and December–January–February (DJF) mean percent changes in temperature metrics under RCP8.5, GLENS, GEQ, Solar3x3, Solar1x1 ensemble mean (2075–2095) and GEOHEATS ensemble mean relative to the baseline ensemble mean (RCP8.5 runs during 2010–2030).

	Change relative to the baseline	Tropical static stability	Meridional temperature gradient	Subtropical tropopause height	T1_surface	T1_troposphere
JJA	RCP8.5	10.7 ± 0.2%	−4.0 ± 0.7%	4.0 ± 0.2%	9.6 ± 0.4%	4.4 ± 0.4%
	GLENS	−1.0 ± 0.1%	3.8 ± 0.4%	−6.7 ± 0.1%	1.1 ± 0.2%	−1.0 ± 0.2%
	GEQ	−2.7 ± 0.2%	2.4 ± 0.8%	−9.8 ± 0.2%	−0.1 ± 0.4%	1.5 ± 0.4%
	Solar3x3	−1.6 ± 0.2%	−0.2 ± 0.7%	−0.1 ± 0.1%	−2.2 ± 0.3%	−3.6 ± 0.4%
	Solar1x1	−2.7 ± 0.2%	0.9 ± 0.6%	−0.9 ± 0.1%	2.9 ± 0.3%	2.4 ± 0.3%
	GEOHEATS	0.9 ± 0.2%	1.6 ± 0.6%	−6.1 ± 0.1%	1.8 ± 0.3%	1.2 ± 0.3%
DJF	RCP8.5	9.1 ± 0.2%	−7.8 ± 0.6%	3.6 ± 0.2%	−23.2 ± 0.7%	−13.9 ± 0.8%
	GLENS	−0.5 ± 0.1%	1.2 ± 0.3%	−7.1 ± 0.1%	0.5 ± 0.3%	4.2 ± 0.4%
	GEQ	−2.5 ± 0.2%	−4.0 ± 0.6%	−9.8 ± 0.2%	0.1 ± 0.7%	5.9 ± 0.8%
	Solar3x3	−1.0 ± 0.2%	−0.1 ± 0.6%	−0.9 ± 0.2%	−2.0 ± 0.6%	2.3 ± 0.7%
	Solar1x1	−4.2 ± 0.2%	−4.4 ± 0.5%	−0.6 ± 0.2%	−15.7 ± 0.7%	−8.9 ± 0.9%
	GEOHEATS	1.2 ± 0.2%	−0.2 ± 0.5%	−3.0 ± 0.1%	−0.6 ± 0.5%	−0.3 ± 0.6%

Percent changes represent the experiment minus the baseline divided by the baseline value. ± range that indicates the standard error in estimating the change.

height in GEQ during these two seasons. However, the reduction of subtropical tropopause height decreases to 7% in GLENS, which is associated with less stratosphere warming and less troposphere cooling in GLENS than that in GEQ. Under Solar3x3 and Solar1x1, decreases in subtropical tropopause height are less than 1% due to tropical tropospheric overcooling but without additional stratospheric heating.

Meridional mass stream functions

We first examine the climatology of the meridional mass stream function (ψ_m) calculated for the individual ensemble members and then averaged for the ensemble mean. The absolute meridional mass stream function simulated in the baseline period and its changes in the perturbed experiments are shown in Fig. 2. Climatologically, there is a clockwise rotation in the Northern Hemisphere HC and an anticlockwise rotation in the Southern Hemisphere, with a stronger rotation and a wider latitude span in winter than in summer. Relative to the baseline, RCP8.5 shows increased overturning in the upper troposphere in both the northern and southern HCs in the winter season, which is likely a consequence of the rise in subtropical tropopause height due to GHGs[12] (Figs. 1 and 2). The negative $\psi_m$anomalies (shading) at lower levels appear over 10°S–20°N during DJF, indicating a significant weakening of the HC. In JJA, the ψ_m anomalies between 400 and 700 hPa are significant and negative over 10°S to the equator; this indicates a slight strengthening of the HC intensity, which is consistent with the previous studies[13].

Both GLENS and GEQ geoengineering ensembles overcompensate for the change in intensity in the upper part of the HC relative to the baseline. This is also the case in GEOHEATS (Supplementary Fig. 2), which suggests the role of the tropical lower stratospheric warming in driving the response[45]. In JJA, there is a weakened overturning in both upward and downward branches of southern HC under GLENS. The reductions of vertical velocities also appear in the upward and downward branches of the southern HC under the Solar3x3 and GEOHEATS cases, respectively, which suggests that stratospheric heating and tropospheric temperature response both contribute the HC weakening due to enhanced stratospheric aerosol concentrations. Under GEQ, there is a similar response of the southern HC overturning to that under GLENS, but the magnitude of the vertical velocities reductions in the downward branch is greater in GEQ than that under GLENS, which is consistent with stronger stratospheric heating in GEQ. The change in vertical velocities is not statistically significant in the middle of the troposphere during 10°S–10°N under GEQ, considering that weakened overturning from stratospheric heating could be offset by enhanced circulation velocities from tropical troposphere temperature profile response of due to reduced insolation under GEQ. The enhanced circulation velocities are expected to appear in the middle of the troposphere during 10°S–10°N under Solar1x1.

In DJF, there is an enhanced overturning in the upward branch of the northern HC and a weakened overturning in the downward branch under GLENS, relative to the baseline. The increases in vertical velocities appear in the upward branch of the northern HC under the Solar3x3 case, and there are reductions in downward overturning under GEOHEATS. However, changes in vertical velocities under GLENS are not statistically significant ~10°N between 900 and 200 hPa, where the climatological average of vertical velocities is roughly maximum in the northern HC. So, the northern HC intensity is expected to vary slightly change under GLENS. Under GEQ, there is a similar response of the northern HC overturning to that under GLENS, but the magnitude of the vertical velocities changes is over 30% greater than that under GLENS, which is consistent with stronger stratospheric heating and tropospheric overcooling in GEQ. Besides, there are statistically significant decreases in vertical velocities ~10°N between 900 and 200 hPa under GEQ, indicating a reduction in HC intensity of northern HC under GEQ. Some signals of northern HC downward vertical velocities reductions also appear under the GEOHEATS case, indicating a significant reduction in vertical velocities of the downward branch of northern HC is driven by the effect of stratospheric heating.

HC intensity and scaling

Figure 3 shows simulated changes in the HC intensity relative to the baseline diagnosed for each experiment during JJA and DJF, alongside the associated standard errors. HC intensity defined in the methods section mainly reflects seasonal changes in the maximum of ψ_m appearing near 10°S/N. In JJA, southern HC intensity strengthens by 3.6 ± 0.7% under RCP8.5 relative to the baseline (Table 3), which is consistent with some CMIP5 coupled

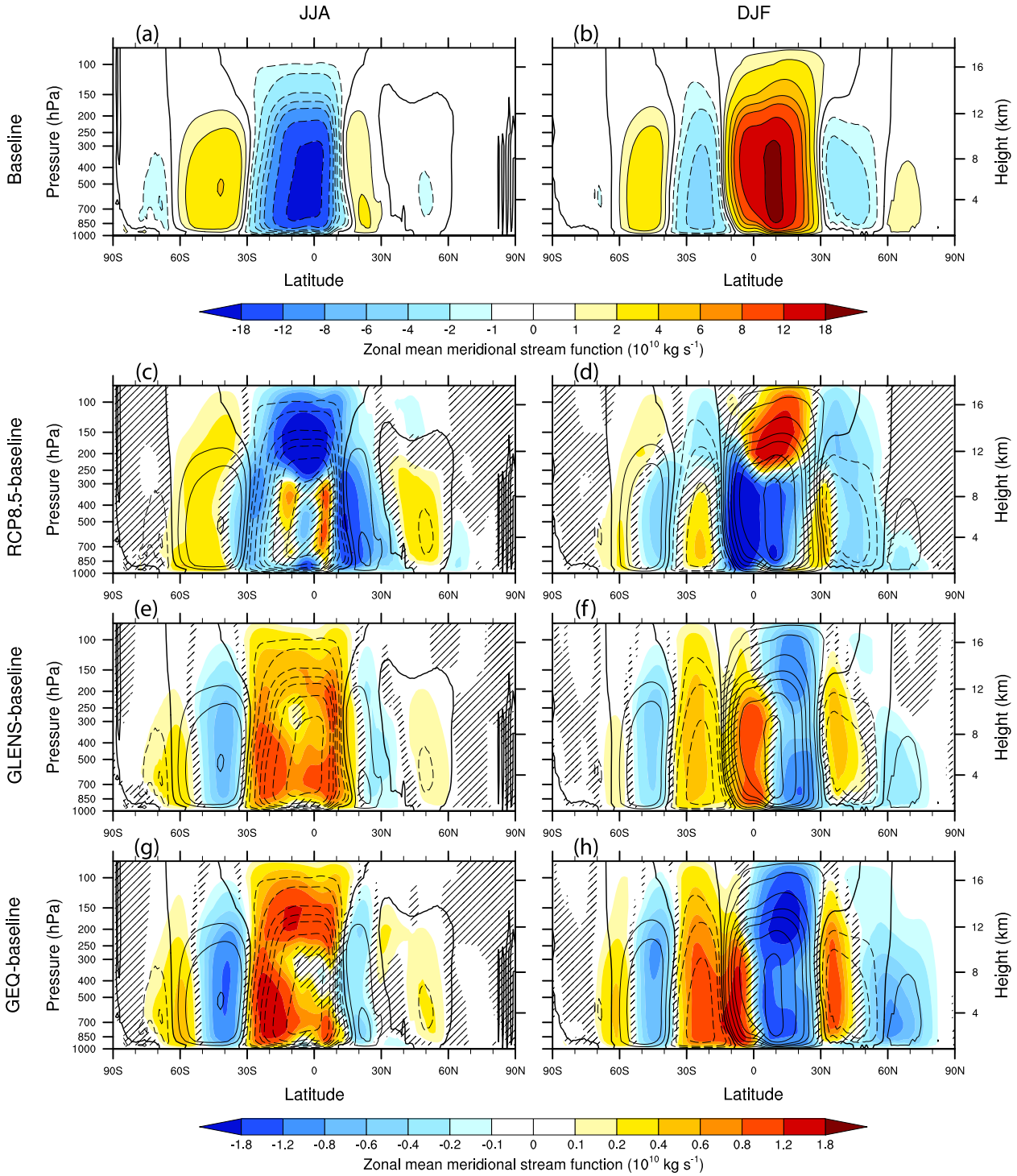

Fig. 2 Zonally seasonal mean meridional mass stream function and its changes. Ensemble and zonal mean JJA (**a**, **c**, **e**, **g**) and DJF (**b**, **d**, **f**, **h**) meridional mass stream function (10^{10} kg s^{-1}) in RCP8.5 averaged over the years 2010–2030 (baseline; **a**, **b**), and anomalies in the RCP8.5 (**c**, **d**), GLENS (**e**, **f**) and GEQ (**g**, **h**) averaged over years 2075–2095, relative to the baseline. Warm colors (positive values) indicate a clockwise rotation and cold colors (negative values) indicate an anticlockwise rotation. Contours indicate the value of seasonal averaged meridional mass stream function (10^{10} kg s^{-1}) in the baseline. Hatched areas are regions where changes are not statistically significant at the 5% level using the Student's *t* test.

models' responses, though the others exhibit a weakening[13]. Geoengineering in GLENS shows an overcompensation of HC intensity in global warming, with a 3.5 ± 0.4% reduction in HC intensity during JJA. Under GLENS, the change in simulated HC intensity is approximately equivalent to the sum of 2.2 ± 0.8% weakening under Solar3x3 and 1 ± 0.7% weakening under GEOHEATS in JJA (Fig. 3). There is a 2.9 ± 0.7% HC intensity weakening under GEQ. The change in HC intensity under GEQ is slightly smaller than that under GLENS, which is associated with no statistically significant change in ψ_m between the equator and 10°S from 300 to 400 hPa. In the above-mentioned simulations, the increases in HC intensity under global warming all are over

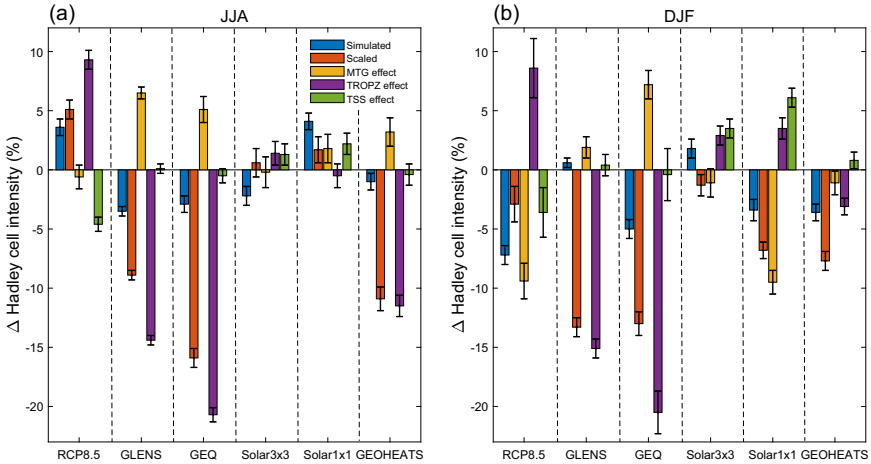

Fig. 3 Changes in simulated and scaled Hadley cell intensity. JJA average (**a**), and DJF average (**b**) ensemble mean percentage changes in winter simulated Hadley cell intensity, scaled HC intensity based on Held[13,15], and the effect from each component on the right-hand side of the Eq. 2 under RCP8.5, GLENS, GEQ, Solar3x3, Solar1x1 ensemble mean (during 2075–2095) and GEOHEATS ensemble mean relative to the baseline ensemble mean (RCP8.5 runs during 2010–2030), respectively. The HC intensity scaling depends on subtropical tropopause height (TROPZ), meridional potential temperature gradient (MTG), and tropical static stability (TSS). To isolate the effect of one component in a perturbation, the other components are set to the baseline values in Eq. 2. Error bars represent standard error. HC intensity is defined as the vertical average of the maximum zonal mean ψ_m between 900 and 200 hPa, see Nguyen et al.[57] for details on the calculation. Since the winter HC is stronger than summer, we only focus on changes in the winter HC intensity, for both hemispheres. Therefore, the analyses are performed on DJF for the Northern Hemisphere and JJA for the Southern Hemisphere separately.

counteracted. However, solar dimming geoengineering in Solar1x1 that maintains the global-mean surface air temperature at the baseline does not mitigate the strengthening in circulation under anthropogenic global warming in JJA.

In DJF, the northern HC weakens by 7.2 ± 0.8% under RCP8.5 relative to the baseline (Table 3). Almost all CMIP5 models are shown by Sea et al.[13] and Vallis et al.[12] to have similar weakening under GHG increases. HC intensity is almost maintained at the baseline value under GLENS, which is consistent with no statistically significant changes in vertical velocities ~10°N between 900 and 200 hPa (Fig. 2). Compared with the baseline, HC intensity decreases by 5.0 ± 0.8% under GEQ, which is associated with 3.6 ± 0.7% reduction under GEOHEATS driven by stratospheric heating. Geoengineering in Solar1x1 partly mitigates the 52% weakening of the northern HC intensity under global warming, while the decrease in HC intensity under global warming is over counteracted with 1.8 ± 0.8% increase in HC intensity under Solar3x3 that maintains not only global-mean surface air temperature, but also the interhemispheric (south-to-north) temperature gradient, and the equator-to-pole temperature gradient at the baseline.

We use the scaling relation based on Held[13,15] (Eq. 2) to estimate HC intensity by the subtropical tropopause height, meridional temperature gradient, and tropical static stability for each geoengineering experiment (Fig. 3). Percent changes represent each perturbation experiment minus the baseline divided by the baseline value, and the range associated with percent standard error. To isolate the effect of one component in a perturbation, the other components are set to the baseline values. The simulated and scaled HC intensities, and the effect of each component on the right-hand side of Eq. (2), can be seen in Supplementary Table 2. Under RCP8.5, the 5.1 ± 0.8% increase in the scaled HC intensity is close to 3.6 ± 0.7% increase in the simulated HC intensity in JJA, which is dominated by the effects of subtropical tropopause height and tropical static stability. In DJF, the −2.9 ± 1.5% reduction in scaled HC intensity under global warming is from the meridional temperature gradient and tropical static stability effects that are partially offset by the subtropical tropopause height effect, which is consistent with the analysis of Seo et al.[13].

In the Solar1x1 simulation, the scaled HC intensity derived from the equation decreases by 6.8 ± 0.7% and increases by 1.7 ± 1.1% relative to the baseline in JJA and DJF, respectively, both of which have the same sign and similar value as the simulated HC intensity. The change in HC intensity is largely affected by the effects of meridional temperature gradient and tropical static stability in JJA, while in DJF, the reduction of HC intensity is mainly from the meridional temperature gradient effect, which is partially counteracted by the effects of subtropical tropopause height and tropical static stability. Under the Solar3x3 case, changes in the scaled HC intensity have different signs from the simulated HC intensity. This is because the changes in meridional temperature gradient are not statistically significant under Solar3x3 relative to the baseline in both seasons; this is associated with effectively meeting T2 goal (Table 2 and Supplementary Table 1), leading to no influence from the meridional temperature gradient in the HC intensity scaling.

Under GLENS and GEQ simulations, the equation of HC intensity indicates a weakening by 9–16%, which is a much greater magnitude than the simulated 3–5% HC intensity reduction in the winter season. It suggests that there is some overestimation of HC intensity reduction using the scaling equation under stratospheric aerosol geoengineering due to strong stratospheric heating, which leads to a 7–10% reduction of subtropical tropopause height. The scaled tropopause height effect for HC intensity is much stronger than the meridional temperature gradient effect or tropical static stability effect in both JJA and DJF due to stratospheric heating under stratospheric aerosol geoengineering; this feature also appears in the GEOHEATS simulations (Fig. 3 and Supplementary Table 2). There are roughly similar meridional temperature gradient effects for HC scaling under GLENS and GEQ in JJA. However, the meridional temperature gradient effect is much smaller in GLENS than in GEQ in DJF, which is related to the effectively controlling equator-to-pole temperature gradient in GLENS. The tropical static stability effect for HC scaling is not statistically significant in both seasons.

ITCZ shift and interhemispheric temperature gradient

The ITCZ is an effective tracer of the latitude of the ascending branch of the HC. The location of the ITCZ gradually varies with

Table 3. JJA average and DJF average ensemble mean changes in winter Hadley cell intensity (%) and ITCZ shift (latitude degree) under RCP8.5, GLENS, GEQ, Solar3x3, Solar1x1 ensemble mean (2075–2095) and GEOHEATS ensemble means relative to the baseline ensemble mean (RCP8.5 runs during 2010–2030), respectively.

Simulations	RCP8.5	GLENS	GEQ	Solar3x3	Solar1x1	GEOHEATS
Δ HC intensity (%)						
JJA	3.6 ± 0.7	−3.5 ± 0.4	−2.9 ± 0.7	−2.2 ± 0.8	4.1 ± 0.7	−1.0 ± 0.7
DJF	−7.2 ± 0.8	0.6 ± 0.4	−5.0 ± 0.8	1.8 ± 0.8	−3.4 ± 0.9	−3.6 ± 0.7
Δ ITCZ (latitude degree)						
JJA	2.65 ± 0.25	−0.72 ± 0.08	0.42 ± 0.19	−0.93 ± 0.15	0.71 ± 0.17	0.40 ± 0.14
DJF	1.06 ± 0.25	−0.16 ± 0.10	−0.83 ± 0.15	−0.04 ± 0.16	0.79 ± 0.16	−0.19 ± 0.14

Percent changes represent the experiment minus the baseline divided by the baseline value. ±range that indicates the standard error in estimating the change. Positive values for ITCZ indicate a northward shift.

the seasons, always towards a warming hemisphere[23]. In JJA, when the ITCZ is located the furthest north ~14.2°N in the baseline, there is a 2.65 ± 0.25° poleward ITCZ migration under RCP8.5 (Fig. 4, Supplementary Fig. 3, Table 3), which shifts toward the warmer hemisphere to transport energy toward the colder hemisphere by the upper branch of HC[51]. Geoengineering in GEQ and Solar1x1 offset the change in ITCZ migration under the global warming scenario by about 85% and 73%, respectively. However, the ITCZ location is over counteracted under GLENS and Solar3x3, with 0.72 ± 0.08° and 0.93 ± 0.15° equatorward migration, respectively. In DJF, when the ITCZ is located the furthest south ~13.7°S in the baseline, there is a 1.06 ± 0.25° northward migration of ITCZ under RCP8.5, which is consistent with a warmer Northern hemisphere. Geoengineering in GLENS and GEQ both overcompensate for the GHG-forced northward ITCZ shifts, producing 0.16 ± 0.10° and 0.83 ± 0.15° southward shifts relative to the baseline, respectively. About 25% of the GHG-forced ITCZ shift is offset by geoengineering in Solar1x1 with 0.79 ± 0.16° northward shift relative to the baseline, which is consistent with ITCZ shifts in G1 solar dimming geoengineering[30,31]. As expected, geoengineering in Solar3x3 generally maintains ITCZ shift under RCP8.5 during DJF.

There are statistically significant biases of seasonal ITCZ locations under the GLENS case relative to the baseline, though the T1 goal is effectively met. In Fig. 4, we consider how the north–south intertropical (30°S–30°N) surface air temperature difference (T1_surface) and the north–south intertropical mean troposphere (200–925 hPa) temperature difference (T1_troposphere) affect the location of ITCZ. Supplementary Table 1 shows the JJA and DJF mean changes in T1_surface and T1_troposphere under these perturbed experiments relative to the baseline together with associated standard errors. The changes in the two metrics look very close under Solar3x3 in JJA and under GEOHEATS in DJF, but the changes in the two metrics are significantly different under the other scenarios and seasons. We find that changes in ITCZ location are slightly better correlated with the changes in T1_troposphere with R values of 0.93 and 0.95 ($p < 0.01$), than for T1_surface with R values of 0.92 and 0.91 ($p < 0.01$), in JJA and DJF respectively (Fig. 4). Based on the linear regression equations in Fig. 4, we calculated the changes in scaled ITCZ using T1_surface and T1_troposphere, separately, shown in Supplementary Fig. 3. In JJA, changes in scaled ITCZ by T1_surface under GLENS and GEQ both have opposite signs with changes in simulated ITCZ. However, the sign of changes in scaled ITCZ by T1_troposphere matches the changes in simulated ITCZ. In DJF, the standard errors of changes in ITCZ scaled by T1_surface under GLENS and GEQ are both greater than those scaled by T1_troposphere, though there is the same sign of change between the scaled and the simulated. Because the change in T1_surface is equivalent to standard error under GLENS, and the change in T1_surface is much smaller than standard error under GEQ. However, changes in T1_troposphere under GLENS and GEQ are both statistically significant (Table 2, Supplementary Table 1).

DISCUSSION

Stratospheric sulfate aerosol geoengineering has been proposed as a potential solution to reduce GHG-induced climate change and its impacts. Here, we investigate changes in the winter HC intensity and the position of ITCZ under geoengineering simulated by CESM1(WACCM). We use two geoengineering ensembles: GLENS with SO_2 stratospheric injections at four different locations, and GEQ with an equatorial injection. To better understand the responses to stratospheric heating, we also compare our results with parallel simulations involving total solar irradiance reductions, and idealized simulations forced by stratospheric heating but without enhanced stratospheric aerosol concentrations.

Relative to the baseline, there is an increase in southern cell intensity in JJA under RCP8.5, which appears in some models e.g., GFDL-CM3, HadGEM2-ES, MRI-CGCM3, NorESM1-ME, etc[13]. Seo et al.[13] investigated the HC intensity using 30 different coupled model simulations in CMIP5 and found that approximately half of the models predict a strengthening of the HC in RCP8.5 during JJA, though the other half exhibited a weakening. On a multi-annual time scale, robust signals of changes in HC intensity caused by increasing GHGs drive a reduction of tropospheric relative humidity and increased frequency of dry months over subtropical and tropical land regions[1]. Geoengineering while GHG concentrations rise in GLENS maintains the three temperature-related metrics, with the pole-equator temperature gradient of particular relevance for the HC. But this results in a weakened HC in JJA relative to the baseline. In DJF, GLENS almost offsets the intensity weakening in RCP8.5. On the other hand, about 30% of the GHG-driven weakening of the northern HC intensity is counteracted under GEQ geoengineering simulations which do not maintain the pole-equator temperature gradient. This partial mitigation is associated with a decrease in tropical static stability which in turn is due to the relative tropical overcooling inherent in the GEQ design[41]. This contrasts with results from an intermediate complexity climate model[32] where sulfate aerosol geoengineering did not mitigate tropical circulation weakening. The different HC intensity responses are associated with climate model responses in tropical tropospheric temperatures to stratospheric aerosols. In addition, the 3.4 ± 0.9% reduction in the Solar1x1 experiment relative to the baseline is consistent with a weakening of the northern HC intensity under the solar dimming G1 scenario relative to piControl[31].

HC intensity reduction using the scaling equation based on Held[13,15] overestimates the simulated HC intensity response under stratospheric aerosol geoengineering. This is associated with the

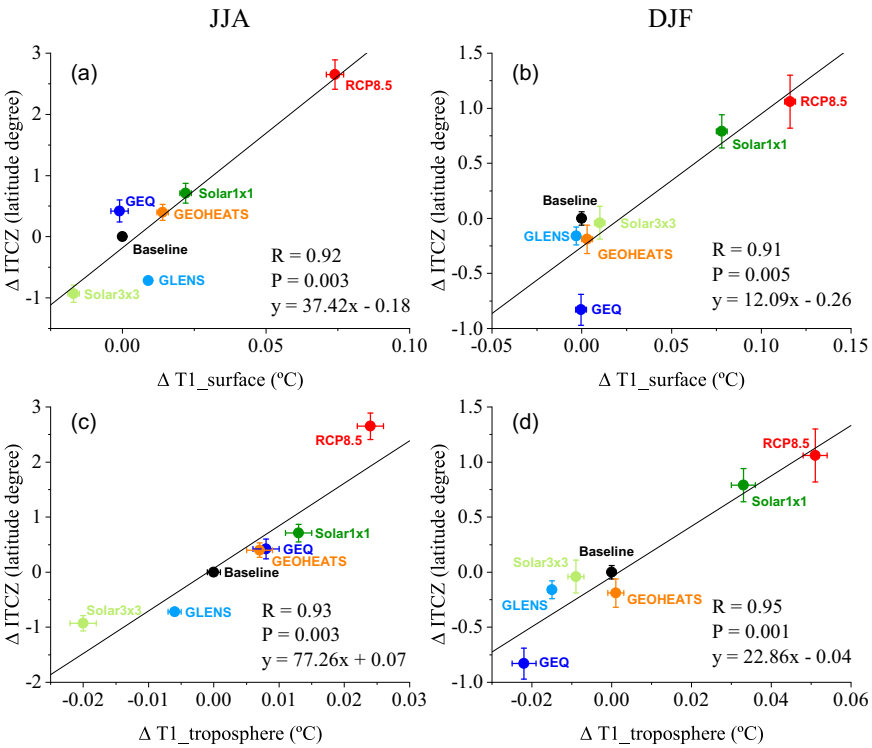

Fig. 4 The relationship between ITCZ shifts and two temperature metrics. Scatter plots of JJA average (**a**, **c**), and DJF average (**b**, **d**) ensemble mean changes in ITCZ, the north–south intertropical (30°S–30°N) surface air temperature difference (T1_surface; **a**, **b**) and the north–south intertropical mean troposphere (200–925 hPa) temperature difference (T1_troposphere; **c**, **d**) under RCP8.5, GLENS, GEQ, Solar3x3, Solar1x1 averaged over years 2075–2095 ensemble mean, and GEOHEATS ensemble mean. Change is relative to the baseline period (RCP8.5, 2010–2030 average). Error bars represent standard error. ITCZ is defined by the latitude closest to the equator where ψ_m vertically averaged between 700 and 300 hPa is zero[58]. Positive values for ITCZ indicate northward shift.

warming of the tropical stratosphere and the cooling of the troposphere due to SAIs[32] leading to a 7–10% reduction of subtropical tropopause height. The strong tropopause height effect also appears in the stratospheric heating simulations, but not in the solar dimming cases. The additional atmospheric heating from the aerosol layer weakens the tropical circulation, suppressing convection and further reducing precipitation[32].

The solar dimming experiment Solar3x3 maintains the three temperature-related metrics at the baseline without stratospheric heating, and GEOHEAT_S case does not include enhanced stratospheric aerosol concentrations but has added stratospheric heating equivalent to the GLENS aerosols. In JJA, the weakening in simulated HC intensity in GLENS relative to the baseline is approximately the sum of the reductions under Solar3x3 and under GEOHEAT_S. Furthermore, the reduced overturning in both upward and downward branches of southern HC under GLENS is also consistent with the upward and downward branches of the southern HC in the Solar3x3 and GEOHEAT_S cases, suggesting that both stratospheric heating and tropospheric temperature response contribute to the HC weakening with SAI geoengineering.

Under RCP8.5, simulated ITCZ location shifts poleward by 2.65° and 1.06° latitude in JJA and DJF, respectively, relative to the baseline. The zonally contrasting shifts of the tropical rain belt driven by increasing GHGs could affect agricultural productivity and food security of billions of people[3,4]. Simulated ITCZ change under both GLENS and GEQ in JJA have opposite signs to changes expected in ITCZ scaled by surface air temperature difference (Supplementary Fig. 3), but agree with the sign of changes scaled by the tropospheric temperatures. In DJF, the uncertainties measured by the standard errors in scaling using the intertropical interhemispheric surface air temperature differences under GLENS and GEQ are also both greater than those scaled by the tropospheric differences. This suggests that changes in the intertropical interhemispheric temperature difference computed in the troposphere are better predictors of ITCZ shifts than the corresponding changes in the intertropical interhemispheric temperature difference at the surface under stratospheric aerosol geoengineering.

By simulation design, both GLENS and GEQ maintain the global-mean temperatures at the baseline levels, and GLENS is also designed to minimize changes in equator-pole temperature gradients. GEQ requires larger rates of SO_2 injection than GLENS which results in stronger stratospheric heating and hence a stronger downward tropospheric impact[36,41,45]. The resulting changes in HC intensity and ITCZ position under GLENS are less than under GEQ during DJF, but not in JJA. Under GLENS, the overcompensation of the HC intensity enhancement under RCP8.5 is slightly larger than that under GEQ in JJA, due to its larger temperature difference across the tropics. GEQ geoengineering under compensates the GHG-forced ITCZ shift in JJA, while GLENS overcompensates, and both are associated with changes in the north–south intertropical mean troposphere temperature difference. The differences in the simulated residual temperature changes in the two geoengineering experiments are direct consequences of the different injection locations and aerosol injection amounts[34].

Our results demonstrate that strategic stratospheric aerosol geoengineering simulated by CESM1(WACCM) can likely reduce changes in the HC intensity and the location of ITCZ under global warming by constraining global-mean surface temperature and its interhemispheric gradients. However, stratospheric sulfate aerosols absorb (near-IR) shortwave radiation and warm the tropical lower stratosphere, thereby leading to up to 7–10% reduction in

subtropical tropopause height. Stratospheric heating and tropospheric temperature response both contribute to the HC weakening due to enhanced stratospheric sulfate aerosol concentrations. It may be possible to devise further strategies that reduce these effects through the use of alternative aerosols that lead to smaller stratospheric heating[52]. The design of strategic SAIs should take into consideration interhemispheric temperature differences both at the surface and in the troposphere for controlling the ITCZ shift.

METHODS

Earth system model and simulations

The geoengineering simulations we analyze here were performed using the Community Earth System Model, version 1, with using the Whole Atmosphere Community Climate Model as its atmospheric component, CESM1(WACCM)[42]. CESM1(WACCM) has been shown to generate a reasonably good representation of the quasi-biennial oscillation, stratospheric ozone column, and water vapor concentrations against present-day observations[42]. Moreover, Mills et al.[42] show that atmospheric aerosol optical depth and surface climate compare well with those observed during the period following the 1991 Mt. Pinatubo eruption, so CESM1 (WACCM) is suitable to conduct stratospheric aerosol geoengineering experiments.

The CESM1 geoengineering Large Ensemble (GLENS) has been used extensively to investigate the climate impacts of SAI, both on the global (e.g., Kravitz et al.,[41]; Tilmes et al.,[34]; Cheng et al.,[36]) and regional scale (e.g., Simpson et al.,[45]; Banerjee et al.,[53]). Regarding the performance of CESM1 model in simulating changes in Hadley circulation (HC), the low–top version of CESM1 (i.e., CESM1-CAM5, up to ~2 hPa) participated in CMIP5 multi-model studies of changes in HC intensity (e.g., Seo et al.,[13]) and tropical width (e.g., Grise et al.,[54]) under increasing GHGs. In both cases, there was a large qualitative and quantitative spread in the trends in these characteristics among the CMIP5 models, and the CESM1 results fell within the general inter-model spread. This suggests that the high-top CESM1 (WACCM) model employed in this study should also perform adequately in simulating changes in the HC. The use of a single model in a relatively large model ensemble reduces the role of natural interannual variability in contributing to the diagnosed HC changes (e.g., Grise et al.,[54]).

We evaluated two sets of simulations involving SO_2 injection into the lower stratosphere (Table 1). The first set involves a 20-member ensemble with annual adjustment of the amount of stratospheric SO_2 injection at four different latitudes (15°N/S and 30°N/S) to maintain three temperature-related metrics T0, T1, and T2 at the baseline present-day levels, which is defined as the average of a 20-member ensemble of 2010–2030 under RCP8.5 conditions[55]. This set of simulations is available to the research community as the GLENS[34]. The second set of simulations involves a 3-member ensemble of annually varying injections only at the equator to offset changes in T0 (GEQ)[41].

In addition, we evaluated parallel simulations involving total solar irradiance reductions (Table 1) instead of SO_2 injection[56]. The Solar3x3 simulation involves annually varying insolation changes in constant, linear, and quadratic functions of the sine of latitude to maintain T0, T1, and T2 at the baseline levels. The Solar1x1 simulation involves annually varying changes in total solar irradiance (with no latitude dependence) to offset changes in T0. To better understand the responses of HC intensity and ITCZ shift to stratospheric heating, we also compare our results to those from a related set of geoengineering simulations without enhanced stratospheric aerosol concentrations but with added stratospheric heating derived from GLENS also conducted using CESM1 (WACCM): an 80-member ensemble of simulations with a short length of 14 months, termed GEOHEATS (Table 1). Transient effects are negligible for HC studies[31] allowing the short GEOHEATS simulations to be utilized and avoiding the substantial change of stratospheric water vapor that accompanies lower stratospheric heating. Each simulation was run under RCP8.5 forcing and initialized from the 1st of January for the years 2010–2030 of four GLENS members without enhanced stratospheric aerosol concentrations but with additional stratospheric heating tendency imposed, which was derived from GLENS over the period from 2075 to 2095[45].

HC and ITCZ

We use the mass stream function to quantify the mean meridional circulation convective flow. The meridional mass stream function (ψ_m) is defined as follows:

$$\psi_m = \frac{2\pi\, a\cos(\phi)}{g}\int_p^{Ps} \mathbf{v}dp \quad (1)$$

where $\mathbf{v}$ represents the zonal mean meridional wind (m s^{-1}), a is the radius of Earth (m), g is the acceleration due to gravity (9.81 m s^{-2}), p is the pressure (mb), Ps is the surface pressure and ϕ is latitude.

HC intensity is defined as the vertical average of the maximum zonal mean ψ_m between 900 and 200 hPa, see Nguyen et al.[57] for details on the calculation. Since the winter HC is stronger than summer, we only focus on changes in the winter HC intensity, for both hemispheres. Therefore, the analyses are performed on DJF for the Northern Hemisphere and JJA for the Southern Hemisphere separately. ITCZ is defined as the latitude closest to the equator where ψ_m vertically averaged between 700 and 300 hPa is zero[58].

Diagnostics of contributing factors

Two different scaling theories have been suggested to investigate the major factors determining changes in the HC intensity[13]. One scaling theory is based on the conserved axial angular momentum of poleward moving upper-level air in the HC[14], the other scaling has the consideration of the baroclinically unstable shear appearing at the poleward edge of the HC[15]. Seo et al.[13] examined both relations, assuming small perturbations are introduced by GHGs under the RCP8.5 scenario. Under this assumption, both scaling theories predict that the HC intensity is proportional to the subtropical tropopause height and the equator-to-higher-latitude potential temperature gradient, but it is inversely proportional to tropical static stability. Guo et al.[31] examined the relations under solar geoengineering finding little difference in the performance of both, and that both relations tended to overestimate the changes compared with climate model simulations. For simplicity we use just the perturbations given by Seo et al.[13] based on the Held[15] scaling relation:

$$\frac{\delta\psi_m}{\psi_m} \sim \frac{9\delta H}{4H} + 2\frac{\delta\Delta_H}{\Delta_H} - \frac{3\delta\Delta_V}{4\Delta_V} \quad (2)$$

where Δ_H is the meridional temperature gradient defined as $\frac{\theta_{eq}-\theta_{higher\ lat}}{\theta_0}$ which is the tropospheric mean meridional potential temperature gradient with θ_0 denoting the hemispheric troposphere mean potential temperature and θ_{eq} calculated between 10°N and 10°S. We follow Seo et al.[13] in taking $\theta_{higher\ lat}$ as the average potential temperature between 10°–50°N for the Northern hemisphere winter and 10°-30°S for the Southern hemisphere. Potential temperature gradients are defined here as the average between 1000 and 400 hPa. $\Delta_V = \frac{\theta_{300}-\theta_{925}}{\theta_0}$ is the dry static stability of the tropical troposphere between 300 hPa and 925 hPa, over 30°S–30°N. H is the subtropical (20°–40°) tropopause height estimated as the level where the lapse rate decreases to 2 °C km^{-1}.

We use two metrics of differential heating/cooling of the hemispheres to understand how the interhemispheric temperature gradient affects ITCZ shifts. The two metrics are defined by the north–south intertropical (30°S–30°N) surface air temperature difference (T1_surface) and the north–south intertropical mean troposphere (200–925 hPa) temperature difference (T1_troposphere), respectively.

DATA AVAILABILITY

All simulations were carried out on the Cheyenne high-performance computing platform (https://doi.org/10.5065/D6RX99HX), and are available on the Earth System Grid at http://www.cesm.ucar.edu/projects/community-projects/GLENS/, and at https://doi.org/10.7298/z8c9-3p43.

CODE AVAILABILITY

The meridional mass stream function calculation is in NCAR Command Language (NCL) scripts and is available at https://www.ncl.ucar.edu/Document/Functions/Built-in/zonal_mpsi.shtml.

Received: 12 August 2021; Accepted: 22 March 2022;
Published online: 19 April 2022

REFERENCES

1. Lau, W. K. M. & Kim, K.-M. Robust Hadley Circulation changes and increasing global dryness due to CO_2 warming from CMIP5 model projections. *Proc. Natl. Acad. Sci. USA* **112**, 3630–3635 (2015).
2. Fu, R. Global warming-accelerated drying in the tropics. *Proc. Natl Acad. Sci. USA* **112**, 3593–3594 (2015).
3. Mamalakis, A. et al. Zonally contrasting shifts of the tropical rain belt in response to climate change. *Nat. Clim. Chang.* **11**, 143–151 (2021).
4. Wheeler, T. & von Braun, J. Climate change impacts on global food security. *Science* **341**, 508–513 (2013).
5. Hu, Y. & Fu, Q. Observed poleward expansion of the Hadley circulation since 1979. *Atmos. Chem. Phys.* **7**, 5229–5236 (2007).
6. Staten, P. W., Lu, J., Grise, K. M., Davis, S. M. & Birner, T. Re-examining tropical expansion. *Nat. Clim. Chang.* **8**, 768–775 (2018).
7. Davis, N. A., Seidel, D. J., Birner, T., Davis, S. M. & Tilmes, S. Changes in the width of the tropical belt due to simple radiative forcing changes in the GeoMIP simulations. *Atmos. Chem. Phys.* **16**, 10083–10095 (2016).
8. Xia, Y., Hu, Y. & Liu, J. Comparison of trends in the Hadley circulation between CMIP6 and CMIP5. *Sci. Bull.* **65**, 1667–1674 (2020).
9. Staten, P. W., Grise, K. M., Davis, S. M., Karnauskas, K. & Davis, N. Regional widening of tropical overturning: forced change, natural variability, and recent trends. *J. Geophys. Res. -Atmos.* **124**, 6104–6119 (2019).
10. Lu, J., Vecchi, G. A. & Reichler, T. Expansion of the Hadley cell under global warming. *Geophys. Res. Lett.* **34**, L06805 (2007).
11. Ma, J., Xie, S.-P. & Kosaka, Y. Mechanisms for tropical tropospheric circulation change in response to global warming. *J. Clim.* **25**, 2979–2994 (2012).
12. Vallis, G. K., Zurita-Gotor, P., Cairns, C. & Kidston, J. Response of the large-scale structure of the atmosphere to global warming. *Q.J.R. Meteorol. Soc.* **141**, 1479–1501 (2015).
13. Seo, K.-H., Frierson, D. M. W. & Son, J.-H. A mechanism for future changes in Hadley circulation strength in CMIP5 climate change simulations. *Geophys. Res. Lett.* **41**, 5251–5258 (2014).
14. Held, I. M. & Hou, A. Y. Nonlinear axially symmetric circulations in a nearly inviscid atmosphere. *J. Atmos. Sci.* **37**, 515–533 (1980).
15. Held, I. *The general circulation of the atmosphere*. 2000 WHOI GFD Program, Woods Hole Oceanographic Institution, Woods Hole, MA, https://gfd.whoi.edu/gfd-publications/gfd-proceedings-volumes/2000-2/. 54 (2000).
16. Held, I. M. & Soden, B. J. Robust responses of the hydrological cycle to global warming. *J. Clim.* **19**, 5686–5699 (2006).
17. Levine, X. J. & Schneider, T. Response of the Hadley circulation to climate change in an aquaplanet GCM coupled to a simple representation of ocean heat transport. *J. Atmos. Sci.* **68**, 769–783 (2011).
18. Wodzicki, K. R. & Rapp, A. D. Long-term characterization of the Pacific ITCZ using TRMM, GPCP, and ERA-Interim. *J. Geophys. Res. Atmos.* **121**, 3153–3170 (2016).
19. Huang, P., Xie, S.-P., Hu, K., Huang, G. & Huang, R. Patterns of the seasonal response of tropical rainfall to global warming. *Nat. Geosci.* **6**, 357–361 (2013).
20. Byrne, M. P. & Schneider, T. Narrowing of the ITCZ in a warming climate: pPhysical mechanisms. *Geophys. Res. Lett.* **43**, 11,350–11,357 (2016).
21. Xu, Y. & Xie, S.-P. Ocean mediation of tropospheric response to reflecting and absorbing aerosols. *Atmos. Chem. Phys.* **15**, 5827–5833 (2015).
22. Chiang, J. C. H. & Friedman, A. R. Extratropical cooling, interhemispheric thermal gradients, and tropical climate change. *Annu. Rev. Earth Planet. Sci.* **40**, 383–412 (2012).
23. Schneider, T., Bischoff, T. & Haug, G. H. Migrations and dynamics of the intertropical convergence zone. *Nature* **513**, 45–53 (2014).
24. Xian, P. & Miller, R. L. Abrupt seasonal migration of the ITCZ into the summer hemisphere. *J. Atmos. Sci.* **65**, 1878–1895 (2008).
25. MacMartin, D. G., Ricke, K. L. & Keith, D. W. Solar geoengineering as part of an overall strategy for meeting the 1.5 °C Paris target. *Philos. Trans. R. Soc. A-Math. Phys. Eng. Sci.* **376**, 20160454 (2018).
26. National Research Council. *Climate Intervention: Reflecting Sunlight to Cool Earth*. (The National Academies Press, 2015). https://doi.org/10.17226/18988.
27. Robock, A. Volcanic eruptions and climate. *Rev. Geophys.* **38**, 191–219 (2000).
28. Kravitz, B. et al. Climate model response from the Geoengineering Model Intercomparison Project (GeoMIP). *J. Geophys. Res. Atmos.* **118**, 8320–8332 (2013).
29. Tilmes, S. et al. The hydrological impact of geoengineering in the Geoengineering Model Intercomparison Project (GeoMIP). *J. Geophys. Res. Atmos.* **118**, 11,036–11,058 (2013).
30. Smyth, J. E., Russotto, R. D. & Storelvmo, T. Thermodynamic and dynamic responses of the hydrological cycle to solar dimming. *Atmos. Chem. Phys.* **17**, 6439–6453 (2017).
31. Guo, A., Moore, J. C. & Ji, D. Tropical atmospheric circulation response to the G1 sunshade geoengineering radiative forcing experiment. *Atmos. Chem. Phys.* **18**, 8689–8706 (2018).
32. Ferraro, A. J., Highwood, E. J. & Charlton-Perez, A. J. Weakened tropical circulation and reduced precipitation in response to geoengineering. *Environ. Res. Lett.* **9**, 014001 (2014).
33. Kravitz, B. et al. The Geoengineering Model Intercomparison Project (GeoMIP). *Atmos. Sci. Lett.* **12**, 162–167 (2011).
34. Tilmes, S. et al. CESM1(WACCM) Stratospheric Aerosol Geoengineering Large Ensemble (GLENS) Project. *Bull. Am. Meteorol. Soc.* **99**, 2361–2371 (2018).
35. Haywood, J. M., Jones, A., Bellouin, N. & Stephenson, D. Asymmetric forcing from stratospheric aerosols impacts Sahelian rainfall. *Nat. Clim. Chang.* **3**, 660–665 (2013).
36. Cheng, W. et al. Soil moisture and other hydrological changes in a stratospheric aerosol geoengineering large ensemble. *J. Geophys. Res. Atmos.* **124**, 12773–12793 (2019).
37. Bala, G. & Caldeira, K. Geoengineering Earth's radiation balance to mitigate CO2-induced climate change. *Geophys. Res. Lett.* **27**, 2141–2144 (2000).
38. Kravitz, B., MacMartin, D. G., Wang, H. & Rasch, P. J. Geoengineering as a design problem. *Earth Syst. Dynam.* **7**, 469–497 (2016).
39. Bekryaev, R. V., Polyakov, I. V. & Alexeev, V. A. Role of polar amplification in long-term surface air temperature variations and modern arctic warming. *J. Clim.* **23**, 3888–3906 (2010).
40. Pithan, F. & Mauritsen, T. Arctic amplification dominated by temperature feedbacks in contemporary climate models. *Nat. Geosci.* **7**, 181–184 (2014).
41. Kravitz, B. et al. Comparing surface and stratospheric impacts of geoengineering with different SO2 injection strategies. *J. Geophys. Res. Atmos.* **124**, 7900–7918 (2019).
42. Mills, M. J. et al. Radiative and chemical response to interactive stratospheric sulfate aerosols in fully coupled CESM1(WACCM). *J. Geophys. Res. Atmos.* **122**, 13,061–13,078 (2017).
43. Ferraro, A. J., Highwood, E. J. & Charlton-Perez, A. J. Stratospheric heating by potential geoengineering aerosols. *Geophys. Res. Lett.* **38**, L24706 (2011).
44. Richter, J. H. et al. Stratospheric dynamical response and ozone feedbacks in the presence of SO2 injections. *J. Geophys. Res. Atmos.* **122**, 12,557–12,573 (2017).
45. Simpson, I. R. et al. The regional hydroclimate response to stratospheric sulfate geoengineering and the role of stratospheric heating. *J. Geophys. Res. Atmos.* **124**, 12587–12616 (2019).
46. Richter, J. H. et al. Stratospheric response in the first geoengineering simulation meeting multiple surface climate objectives. *J. Geophys. Res. Atmos.* **123**, 5762–5782 (2018).
47. Driscoll, S., Bozzo, A., Gray, L. J., Robock, A. & Stenchikov, G. Coupled Model Intercomparison Project 5 (CMIP5) simulations of climate following volcanic eruptions. *J. Geophys. Res. Atmos.* **117**, D17105 (2012).
48. Robock, A. & Mao, J. Winter warming from large volcanic eruptions. *Geophys. Res. Lett.* **19**, 2405–2408 (1992).
49. Henry, M. & Merlis, T. M. Forcing dependence of atmospheric lapse rate changes dominates residual polar warming in solar radiation management climate scenarios. *Geophys. Res. Lett.* **47**, e2020GL087929 (2020).
50. Govindasamy, B., Caldeira, K. & Duffy, P. B. Geoengineering Earth's radiation balance to mitigate climate change from a quadrupling of CO2. *Glob. Planet. Change* **37**, 157–168 (2003).
51. Kang, S. M., Shin, Y. & Xie, S.-P. Extratropical forcing and tropical rainfall distribution: energetics framework and ocean Ekman advection. *npj Clim. Atmos. Sci.* **1**, 1–10 (2018).
52. Keith, D. W., Weisenstein, D. K., Dykema, J. A. & Keutsch, F. N. Stratospheric solar geoengineering without ozone loss. *Proc. Natl. Acad. Sci. USA* **113**, 14910–14914 (2016).
53. Banerjee, A. et al. Robust winter warming over Eurasia under stratospheric sulfate geoengineering – the role of stratospheric dynamics. *Atmos. Chem. Phys.* **21**, 6985–6997 (2021).
54. Grise, K. M. et al. Recent tropical expansion: natural variability or forced response? *J. Clim.* **32**, 1551–1571 (2019).
55. Kravitz, B. et al. First simulations of designing stratospheric sulfate aerosol geoengineering to meet multiple simultaneous climate objectives. *J. Geophys. Res. Atmos.* **122**, 12,616–12,634 (2017).
56. Visioni, D., MacMartin, D. G. & Kravitz, B. Is turning down the sun a good proxy for stratospheric sulfate geoengineering? *J. Geophys. Res. Atmos.* **126**, e2020JD033952 (2021).
57. Nguyen, H., Evans, A., Lucas, C., Smith, I. & Timbal, B. The hadley circulation in reanalyses: climatology, variability, and change. *J. Clim.* **26**, 3357–3376 (2013).

58. Byrne, M. P., Pendergrass, A. G., Rapp, A. D. & Wodzicki, K. R. Response of the intertropical convergence zone to climate change: location, width, and strength. *Curr. Clim. Chang. Rep.* **4**, 355–370 (2018).
59. Kravitz, B., MacMartin, D. G., Wang, H. & Rasch, P. J. Geoengineering as a design problem. *Earth Syst. Dynam* **7**, 469–497 (2016).
60. Simpson, I. R. et al. The regional hydroclimate response to stratospheric sulfate geoengineering and the role of stratospheric heating. *J. Geophys. Res. Atmos.* **124**, 12587–12616 (2019).

ACKNOWLEDGEMENTS

This research was supported by the National Key Research and Development Program of China (Grant no. 2016YFA0602500). Data analysis and technical validation were partially funded by the Strategic Priority Research Program of Chinese Academy of Sciences (Grant no. XDA23070400), the state key program of National Natural Science Foundation of China (Grant no. 91425303; Grant no. 71533004), and the National Program on Key Research Project (Grant no. 2017YFA0603703). Support was provided in part by the National Science Foundation through agreements CBET-1818759, CBET-1931641, CBET-2038246. Kravitz was supported by the Indiana University Environmental Resilience Institute, and the *Prepared for Environmental Change* Grand Challenge initiative. Visioni was supported by the Atkinson Center for a Sustainable Future at Cornell University. Cheng was supported by the research start-up project for new recruits at Institute of Geographic Sciences and Natural Resources Research, CAS. The Pacific Northwest National Laboratory is operated for the U.S. Department of Energy by Battelle Memorial Institute under contract DE-AC05-76RL01830. The authors would like to thank I.R. Simpson, S. Tilmes, and T.R. Ault for the manuscript revision.

AUTHOR CONTRIBUTIONS

W.C., D.M., and B.K. designed the research. W.C., D.V., I.S., and L.H. performed the simulations and data analysis. W.C. drafted the manuscript. D.M., B.K., D.V., E.B., Y.X., I. S., Y.L., L.H., Y.H., P.S., P.H., J.M., A.G., and X.D. revised the manuscript.

COMPETING INTERESTS

The authors declare no competing interests.

ADDITIONAL INFORMATION

Supplementary information The online version contains supplementary material available at https://doi.org/10.1038/s41612-022-00254-6.

Correspondence and requests for materials should be addressed to Wei Cheng, Douglas G. MacMartin or Xiangzheng Deng.

Reprints and permission information is available at http://www.nature.com/reprints

Publisher's note Springer Nature remains neutral with regard to jurisdictional claims in published maps and institutional affiliations.